[Proc. SPIE/SPSE Vol. 1658, "Nonlinear Image Processing III", pp. 151–164, San Jose CA, February 1992]

Application of Morphology to Feature Extraction for Face Recognition

Gaile G. Gordon*
TASC, 55 Walkers Brook Drive, Reading, MA 01867

Luc Vincent*
Xerox Imaging Systems, 9 Centennial Drive, Peabody, MA 01960

Abstract

This paper explores the use of morphological operators for feature extraction in range images and curvature maps of the human face. We describe two general procedures. The first is the identification of connected part boundaries for convex structures, which is used to extract the nose outline and the eye socket outlines of the face. The part boundaries are defined locally based on minima of minimum principal curvature on the surface. The locus of these points suggests boundary lines which surround most convex regions on the surface. However, most of these boundaries are not completely connected. To remedy this problem, we developed a general two-step connection procedure: the partial boundaries are first dilated in such a way that the gaps between them are filled. Second, the resulting dilated outlines are skeletonized with the constraint that the pixels belonging to the original boundary parts cannot be removed. A marker which identifies the convex region we are trying to describe is then used to select the region enclosed by the new connected outline. We show examples of this procedure in the extraction of the nose boundary and eye socket boundary.

The second general procedure discussed is the identification of connected ridge lines, which is demonstrated in the extraction of the browline and the chin/jaw line. Ridge lines are defined as local maxima of maximum curvature in the direction of maximum curvature. The same skeleton-based procedure as above is first used to connect the ridge lines. Skeletonization is then used again to reduce these lines to simply connected ones. The last step primarily consists in extracting the longest path within the obtained components: this is achieved by using the *propagation function* to find the extremities of these paths and then connecting them within the components by means of geodesic distance functions. The entire process provides a robust and accurate extraction of brow and chin/jaw lines.

1 Introduction: The Study of Face Recognition

Face recognition is a difficult visual representation task in large part because it requires differentiating among objects which vary only subtly from each other. It represents a particularly interesting case within the context of object recognition. It is much less constrained than the case of rigid machined objects most often considered and yet it is more constrained than the general case which includes "objects" which could be posed in an infinite number of configurations (e.g., a cat or a sweater...). Human face recognition abilities provide convincing proof that the problem can be solved; we have the capacity for remembering and accurately distinguishing among hundreds, maybe even thousands of faces. Yet, despite a long standing interest in the computer vision research community, very little progress has been made toward developing a robust automatic face classification system. Importantly, face recognition is also rich in application areas. The most familiar application is in the security industry. Popular movies and television series have already shown many examples of high security systems which base admittance on identification by face matching. Although the accuracy required for high security applications may not be

*This work was done primarily while the authors were at the Harvard University Robotics Laboratory, Cambridge MA

available in the short term, lower security applications or identification verification systems may be practical in the near future. Other application areas include the field of communications, specifically adaptive image compression for teleconferencing, and the field of advanced human interface, which seeks to use information about the facial expression or identity of the user to adapt interaction paradigms.

Previous research in face recognition has been based primarily on two dimensional (2D) intensity images. This work can be grouped into two categories. The first category involves description of individual features and their relationships. Several different approaches of this type are given by [8, 14, 32, 15, 24, 19]. The second type of approach uses general pattern recognition techniques which do not include processing specific to faces. Examples are given by [26, 9, 1, 3]. Some researchers have tried to improve upon these methods with hybrid systems. These systems tend to use feature extraction to set orientation and bounds for the general pattern recognition techniques [3, 5, 4].

For all but the simplest cooperative subject security application, however, the view angle of a face will not be constrained. Thus, unless many different views of each subject are used in the system, treating the face as a 2D pattern is not sufficient for robust recognition. When comparing among a large number of faces, the multiple view approach becomes impractical. Taking 3D information into account would allow for a single view invariant description, which is more robust and practical for large databases. Depth based processing also has the potential for better accuracy, a richer feature base, and provides the potential to use curvature measures which are inherantly viewpoint invariant [11].

2 Specifications of Range Data

Advances in range finding technology have made it possible to trace the shape of the face at a resolution of 0.4 mm or smaller, making possible accurate calculation of surface curvatures given a careful treatment of noise. The availability of this type of data opens up many new avenues for face recognition using surface description.

The data used in this paper were generated by a rotating laser scanner system. Depth is stored in a cylindrical coordinate system, where $f(\theta, y)$ is distance measured from the central vertical axis to the surface (see figure 1). Each data set has 256 equally spaced samples along the vertical axis, y, and 512 equally spaced samples in θ from 0 to 2π. Figure 2(a) shows an example depth file in parameter space. Figure 2(b) shows a view of the same data set rendered from a polygon model made by connecting nearest neighbors in the depth map. This style of representing range data has many useful properties. Importantly, it gives a panoramic perspective without complex reconstruction techniques. A rotation of the object about the y axis maps to a translation in θ in the parameter space. A translation of the object within the range of the sensor will correspond to an expansion in θ about one of the longitudes in parameter space. The mapping from parameter space to absolute 3D coordinates is straightforward.

3 The Use of Differential Geometry in Surface Description

Information about how a smooth surface is curving is essential in describing natural or free form surfaces such as the face. Curvature of a surface is also a local surface property, and hence is independent of the pose of the surface with respect to the coordinate system of the data. Let us summarize briefly the definition of *principal curvature*, which is the basis for the features we wish to extract.

3.1 Principal Curvature

For the case of a curve in a plane, the most intuitive definition of the curvature κ at a point P on the curve is in terms of the radius of curvature at P, $1/\kappa$. Three points define a unique circle. If we select two points on a given curve, one on either side of P, the radius of curvature is the radius of the circle defined by these points in the limit as the two surrounding points approach P. Curvature can also be defined as the rate of change of the tangent vector field of the curve.

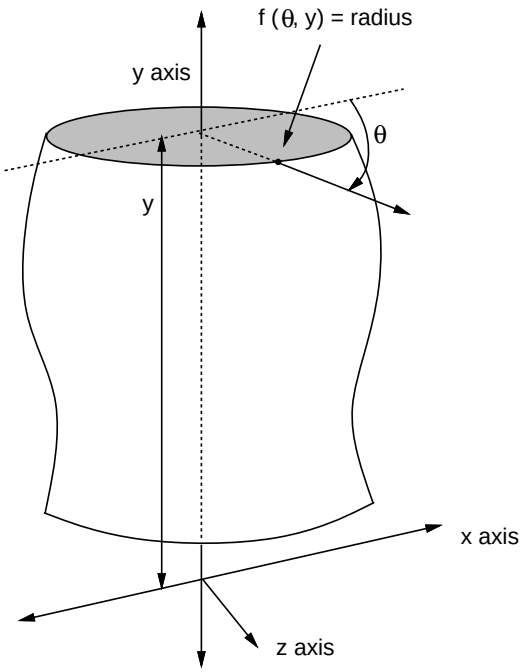

Figure 1 : *Cylindrical parameterization of the depth data.*

These concepts based on plane curves can be extended to describe surfaces. At each point P on the surface (required to be twice continuously differentiable), a curve is formed by the intersection of the surface and the normal plane in a given tangent direction $\vec{t_i}$. The curvature of this planar curve is the normal curvature κ_n at P in the direction $\vec{t_i}$. The maximum and minimum normal curvatures at a point define the *principal curvatures*, κ_{max} and κ_{min}; the directions $\vec{t}_{max}$ and $\vec{t}_{min}$ associated with each principal curvature are the *principal directions* of the surface at P and by Euler's theorem are orthogonal [18].

The principal curvatures and the principal directions are given by the eigenvalues and eigenvectors of the shape operator matrix:

$$L = DG^{-1}, \tag{1}$$

where D is the second fundamental form of the surface and G is the first fundamental form. These fundamental forms can be calculated as functions at each point of the first and second differences of the sampled surface data. For a more detailed background in differential geometry consult [18].

3.2 Ridge and Valley lines

Important surface structure is conveyed by extrema in principal curvatures κ_{max} and κ_{min}. To capture this information, we define two new features, ridge and valley lines. Ridge lines are defined as local maxima in κ_{max} along the line of maximum curvature ($\vec{t}_{max}$) and similarly valley lines are local minima in κ_{min} along line of minimum curvature ($\vec{t}_{min}$). For practical computation we also apply thresholds, $thresh_r$ and $thresh_v$.

Thus to calculate the ridge lines we

- consider only ($k_{max} > thresh_r$),
- using bilinear interpolation among the local neighbors of each pixel, suppress all points which are not local maxima along the line of maximum curvature $\pm\vec{t}_{max}$.

Valley lines are found with a similar process. The threshold applied is instead ($k_{min} < thresh_v$), and points are suppressed when they are not local minima in direction $\pm\vec{t}_{min}$. It is important to note that setting the thresholds

(a)

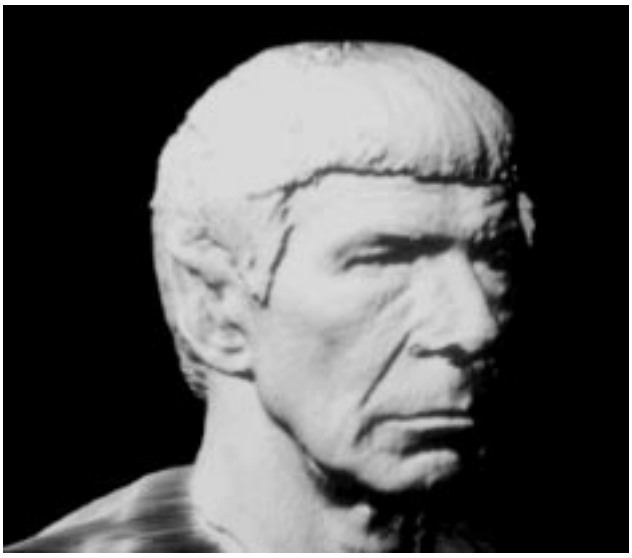

(b)

Figure 2 : *(a) Depth of face parameterized as $f(\theta, y)$ (Leonard Nimoy as Spock), (b) rendered polygonal model of face composed from coarse sampling of depth data.*

in this case is not the sensitive process it is in edge detection. These thresholds are absolute measurements related to the physical structure of the surface. We can set the same threshold across all images. With faces, for instance, curvature at the magnitude of the nose is significant, whereas curvature at the magnitude of skin imperfections of small wrinkles is not interesting for most applications.

Figure 3 shows ridge and valley lines for two faces. Note how clearly the characteristic features of the face are displayed by these extrema.

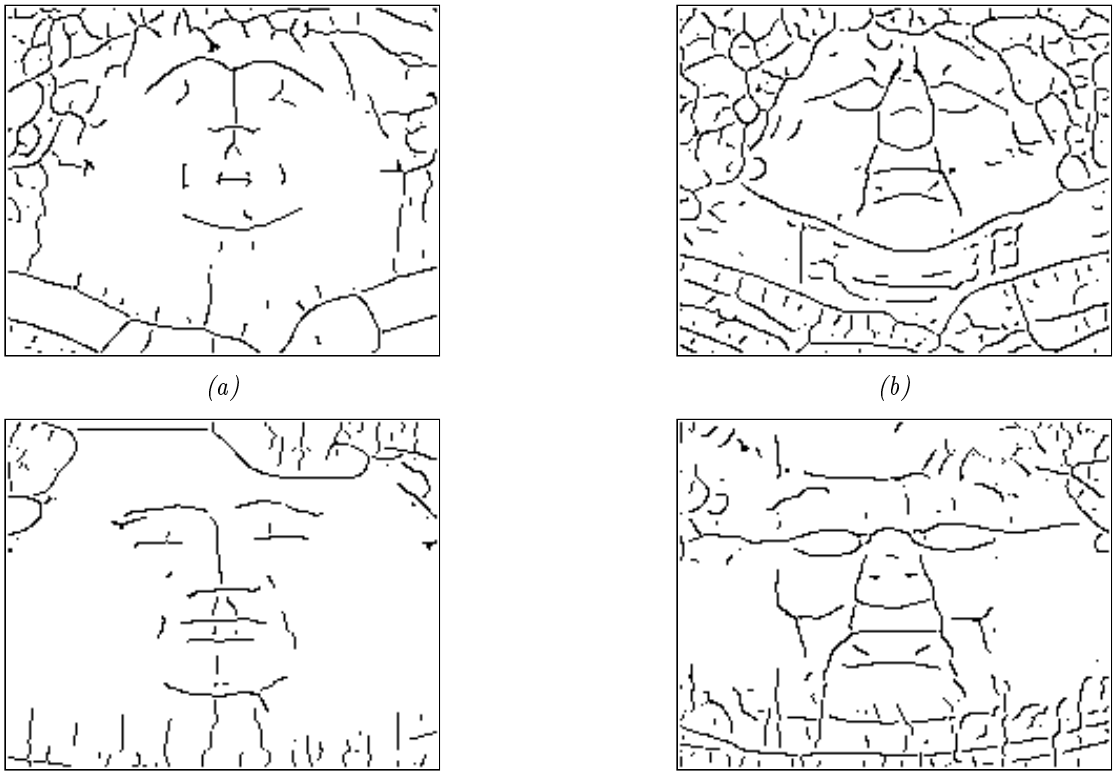

Figure 3: *(a)(c) Ridge lines: local maxima of* $(k_{max} > thresh_r)$ *in direction of maximum curvature, and (b)(d) valley lines: local minima of* $(k_{min} < thresh_v)$ *in direction of minimum curvature. (a) and (b) are from subject 1, (c) and (d) from subject 2. Data is presented as* $f(\theta, y)$

3.3 Correspondence of ridge and valley lines to physical features

The correspondence of ridge lines as we have defined them to physical features of a "ridge" is very intuitive. If any area on the surface is elevated relative to its surroundings it will have a crest or ridge of some form at its peak. If the area is elongated, the ridge will form a connected line. These points, as extrema of curvature, are well defined and useful for registration and description of the surface.

Valley lines as we have defined them also have an intuitive correspondence to the physical feature we usually refer to as a "valley", a depressed region in a surrounding plateau. More importantly for many applications, they also are found surrounding any compact convex region. This point is related to the definition Hoffman and Richards [13] gave for part boundaries [11]. It is this configuration of valley lines, enclosing a convex structure, which we are interested in locating in our data. We discuss this in the next section. Then, in § 5, we discuss the extraction of features in ridge line images.

Note that once the desired features have been extracted from binary images of valley and ridge lines, they can be

mapped back onto the original 3D model. This allows us to numerically describe these features by means of absolute measurements. For example, the width of the chin is obtained as the distance *in 3D space* between the extremities of the extracted chin line. Other parameters, like the width of the nose or the length of the brow line can be obtained in a similar manner.

4 Features marked by configuration of valley lines

Although close in some cases, it is important to note that valley lines surrounding convex regions are not generally completely connected boundaries. A major problem is that, unlike the zero crossings of a function, connecting local minima of lines of curvature will create curves which can end abruptly with no continuation. This occurs when a local minimum and a local maximum on one line of curvature coalesce and disappear in nearby lines of curvature. Combined with *a priori* knowledge of the face, however, this information can become very useful. If we know what we are looking for we can use this information to help fill in the gaps and identify significant boundary points using morphology [22, 23]. We illustrate this with the calculation of eye socket regions and the bounding area for the nose.

4.1 Extraction of eye socket regions

For the eye regions, we first use the location of the corner cavities of the eyes (or approximations based on the eyeball location if the cavities were not located successfully)[12] to establish a region of interest for the search. All further processing can be done within this bounding area, speeding up the process considerably. An example is shown by the rectangle superimposed on figure 4(a).

As already mentioned and as can be seen on figure 4(b), the main difficulty we encounter is to connect the different pieces of the boundary of these eyesocket regions. Connection techniques based on neighborhood graphs, like the Gabriel Graph [10] or the Relative Neigborhood Graph [25] are inappropriate here, since they do not account for the fact that gaps between boundary parts are relatively small. These graphs would thus yield numerous wrong connections. Similarly, graph-based techniques like those proposed in [21] would be too global in nature.

For these reasons, we developed a new connection procedure, which we also used in the extraction of nose regions (see § 4.2) as well as features marked by configurations of ridge lines (see § 5). It consists of the following succession of operations:

- First dilate the image by a small isotropic structuring element. Since the gaps between contour parts are not too large, this transformation has the effect of reconnecting the eye-socket region correctly (see figure 4(c)). The structuring element used for this process is a discrete disc of radius 2, i.e. an elementary octagon.
- The contours resulting from this dilation operation need to be thinned. At this point, one cannot simply erode these contours again by the same disc (thus performing a closing of the original image), since some of the disconnections could still remain afterwards! Instead, we based our approach on the binary skeleton transformation [2, 6]. It has the advantage of yielding a 1-pixel thickness contour while preserving the homotopy (i.e. here, the connectivity) of the dilated contours. However, using a classical skeleton transformation often produces parasitic barbs, which then need to be pruned. In addition, the resulting pruned skeleton may not contain the original contour parts any more.

  To avoid these problems, we used an algorithm originally proposed in [27, 28], which can be seen as a constrained skeleton algorithm: the previously obtained thick contours are progressively thinned starting from their boundary pixels. Two constraints are used during this operation:

  – A pixel can be removed only if this removal does not modify the *homotopy* of the current set of pixels, i.e. does not break a line or remove a connected component.

  – A pixel belonging to the original contour (the broken valley lines) cannot be removed.

  This process is iterated until stability (no more thinning is possible under the constraints). Its result is a superset of figure 4(b), where the components which had been connected via dilation are now connected by a

1-pixel thickness line (see figure 4(d)). Note that the entire process is extremely fast, since the algorithm is based on a breadth-first propagation inside the dilated components, and is implemented via a queue of pixels [27, 29].

More generally, this connection technique can be used to nicely connect components of a binary image which are "relatively close to one another". The closeness of two components can be defined in various ways depending on the structuring element used in the initial dilation step.

The next stage of the algorithm is to determine which of the boundary points specify the eyesocket itself. This can be done rather straightforwardly by using a previously extracted marker of the eyeball or lid [12]. This marker is shown in figure 4(e). Using a morphological *seedfill* algorithm known as geodesic reconstruction [16], we can now extract the connected component of the background (inverted figure 4(d)) which is "marked" by this lid. This yields the region illustrated by figure 4(f). The external boundary of this region is the boundary of the desired eyesocket (see figure 4(g)).

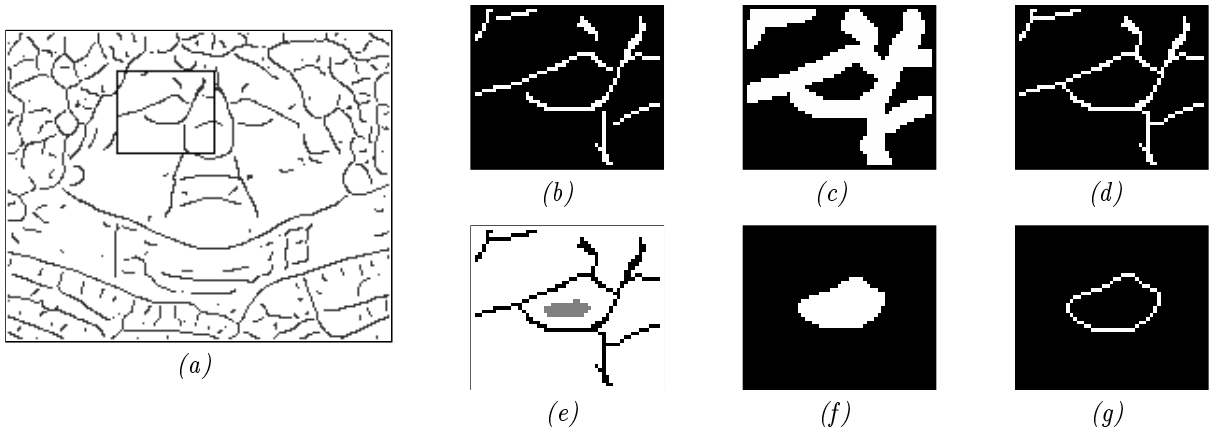

Figure 4 : *Sequence of images illustrating the extraction of the eyesocket regions*

4.2 Extraction of nose region

A similar technique allows us to extract the nose region. In this process it is common to find more than one nose marker, since the nose ridge often exhibits a "dip" in its middle, thereby yielding two convex regions below and above the dip (see figure 5(a)). We connect the broken boundary with the same process as is used for the eyesocket, and extract the enclosed regions marked. After this reconstruction, an elementary morphological closing is used to connect the extracted regions into one single nose region (see figures 5(b)–(c)), whose boundary is shown figure 5(d).

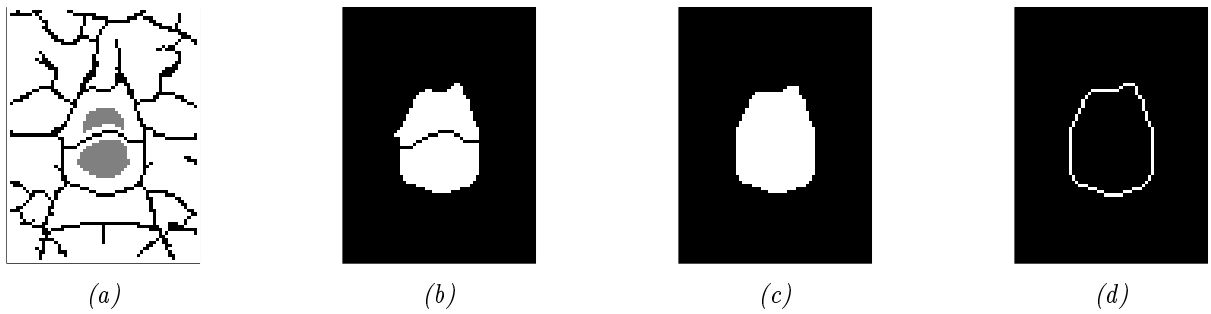

Figure 5 : *Sequence of images illustrating the extraction of the nose region*

5 Features marked by configuration of ridge lines

We shall illustrate the detection of features marked by configurations of ridge lines on the extraction on chin/jaw line and the eyebrow lines. Sample original ridge images are shown in Figure 6.

Figure 6 : *Sample ridge line images used to illustrate the extraction of the chin/jaw line and the eyebrow lines.*

As can be observed on this figure:

1. There are numerous irrelevant ridge lines, primarily oriented vertically.
2. The desired lines are roughly horizontal.
3. The desired lines are not necessarily connected, but the disconnection between their different parts are small.
4. The left and right sides of the chin/jaw ridge never curve downward when the face is in the upright position.

In addition, we can use anthropometric data collected from a wide sample set of human faces [7] to set limits on the location of most facial features relative to other (previously extracted) features. We can find the expected position of the brow and chin lines from the location of

- inside and outside corners of the eyes,
- nose bridge and base,

which are extracted with other processes [12]. The expected position can be expressed in the form of a bounding rectangle. The bounding boxes corresponding to the chin and the eyebrows lines for figure 6(b) are shown in Figure 7(a).

The mainly horizontal orientation of the ridge lines we wish to extract makes it possible to easily filter out a great deal of the noise present on figures 6(a)–(d). A binary opening with a 2 pixel wide horizontal segment

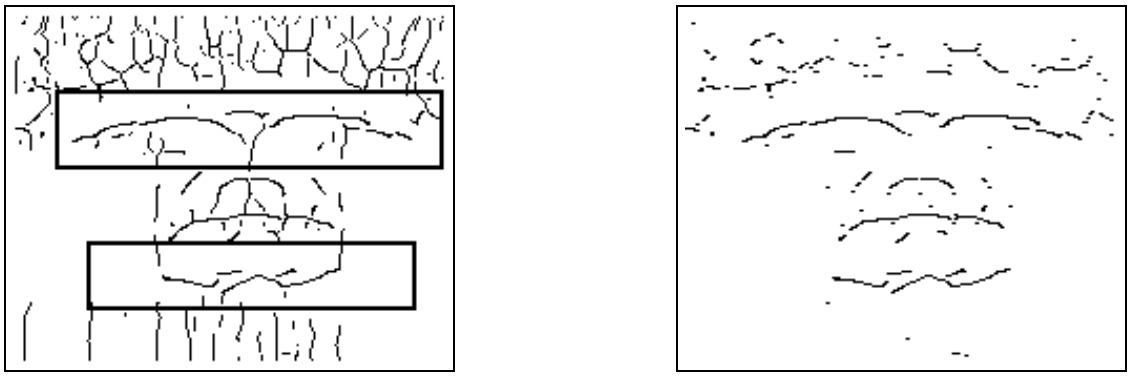

(a) *(b)*

Figure 7: *(a) Bounding rectangles containing the desired ridge lines. (b) After filtering out the ridge lines with the wrong orientation.*

eliminates every line portion whose orientation θ is not within the bounds $[-arctg(1/2); arctg(1/2)]$. The result of this morphological filter for figure 6(b) is shown in Figure 7(b).

The second step of our ridge line extraction method consists in connecting the ridge lines which exhibit small disconnected parts. This is realized by using again the connection technique introduced in § 4. A dilation of figure 7(b) with respect to a discrete disc of size 2 produces a coarse connection of our ridge lines (see figure 8(a)). The second part of the algorithm is the constrained skeleton of figure 8(a), which yields the connected ridge lines shown in Figure 8(b).

At this point, one can notice that the original connection by dilation induces a number of "bridges" between ridge parts, sometimes creating *holes* in the connected ridge lines. These holes are then of course preserved in the homotopic constrained skeletonization process! The technique used to eliminate this problem consists of filling the holes in image 8b (in fact, filling the holes only within the bounding boxes of figure 7(a) is sufficient), which yields figure 8(c). Another skeletonization is then used to produce a thin output, shown in figure 8(d).

By intersecting the result of figure 8(d) with the bounding boxes of figure 7(a), we produce figure 9(a). The final extraction steps proceed as follows:

- Extraction of the largest connected component within each bounding rectangle. One of them corresponds to the chin line whereas the other one contains the desired eyebrow line.
- Removal of chin line portions with wrong orientation. Here, we use the fact that the tips of chin line are ascending in all human faces in the upright position. Using the previously extracted symmetry line of the image [11], we are able to find which parts of the chin ridge are on the left and which parts are on the right. To remove the portions with wrong orientation, we then do as follows:
  - Locate and remove the multiple points of the chin line, thus decomposing it into several simple components.
  - Based on the location of its end points, determine the overall orientation of each component, a technique originally used in [31].
  - On the left of the symmetry line of the face, components must have angle of orientation $10° > \theta > -45°$, similarly on the right of the symmetry line, components must have angle of orientation $45° > \theta > -10°$. Components outside these ranges are removed.
  - "Glue" back the remaining pieces together.
- Extraction of the longest path within each component. This is also a multistep operation which is performed as follows:
  - Compute the propagation function of the chin and the eyebrow components. Recall that the propagation function p_X associates with each pixel of a connected set X its geodesic distance (denoted d_X) to the

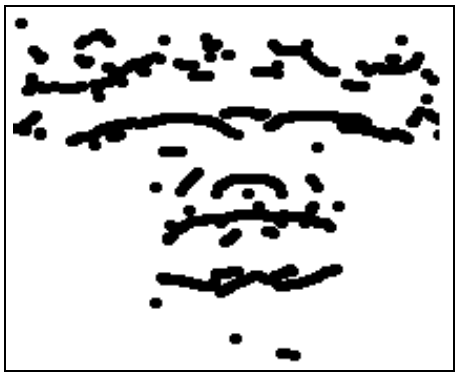

(a) dilation

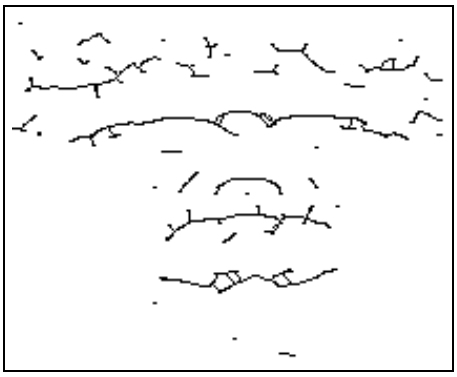

(b) constrained skeleton

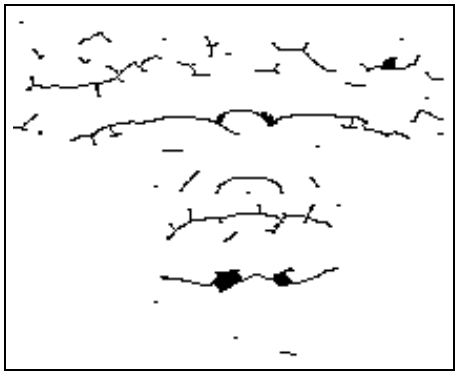

(c) hole filling

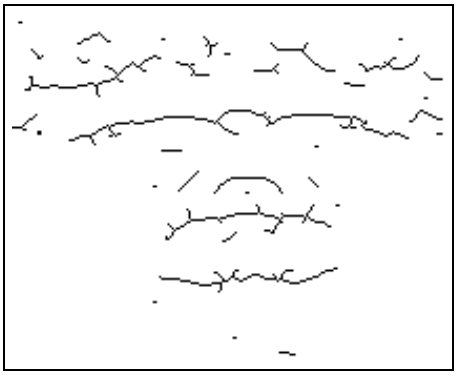

(d) regular 8-connected skeleton

Figure 8 : Connection of ridge lines.

farthest pixel of X:

$$p_X \left(\begin{array}{ccc} X & \longrightarrow & \mathbb{Z}^+ \\ p & \longmapsto & \sup\{d_X(p,q) \mid q \in X\}. \end{array} \right.$$

It turns out to be an extremely useful transformation, whose fast computation was proposed by M. Schmitt a few years ago [20, 17].

- Extract the pixels corresponding to the absolute maximum of the propagation function over each component. These pixels are the end points of the desired longest paths.
- Let X be the considered component, p_1 and p_2 the previously extracted extremities. To find the path connecting these two pixels within X, we use a technique proposed in [30] based on geodesic distance functions [16]. By computing the geodesic distance between every pixel $p \in X$ and p_1 and p_2, we find the pixels $p \in X$ which satisfy:

$$d_X(p,p_1) + d_X(p,p_2) = d_X(p_1,p_2).$$

The locus of these pixels exactly correspond to the desired longest path, as illustrated by figure 9(b).

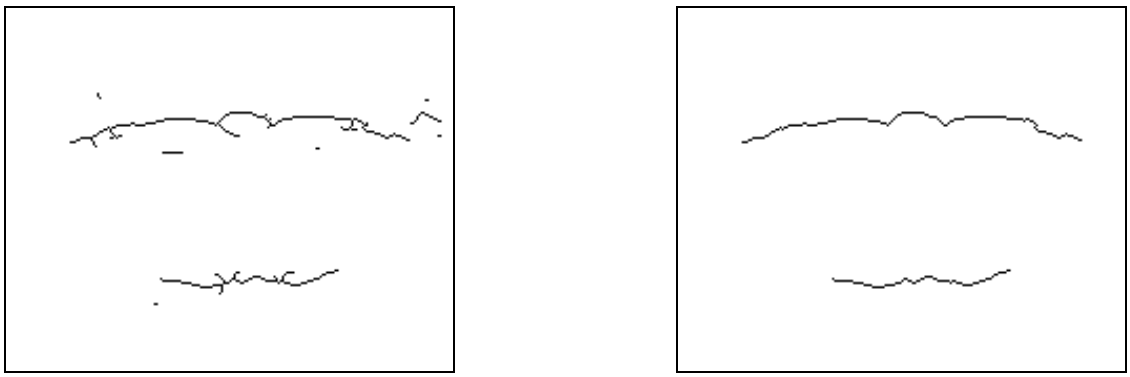

(a) clipped ridge lines *(b) result*

Figure 9 : Final extraction stages for chin and eyebrow lines.

The final chin/jaw and eyebrow lines produced by this technique on the initial ridge images of figure 6 are shown in figure 10.

6 Conclusion

This paper has described general procedures for locating features defined by the configuration of extrema in principal curvature. We have termed these extrema *ridge* and *valley* lines. Such procedures would be useful in any kind of surface registration or description task. Illustrations and examples presented were from the domain of face recognition. We used prior knowledge of the general shape and structure of our surface to generate markers and orientation tuning parameters.

More specifically, we first gave a general procedure for the detection of boundaries of convex markers. This process was illustrated using the examples of the eyesocket and nose regions. It could also be used with different markers to find additional structures of the face such as boundary of lip region. The second type of feature we discussed were orientation specific configurations of connected ridge points, which was illustrated by the extraction of the chin and brow lines. Similarly, this technique could be used with different orientation criteria (and different initial bounds) to find ridge lines of the nose and ears.

A novel connection technique based on the concept of constrained skeleton was also introduced in this paper. It enables us to robustly and precisely reconnect broken lines or broken objects in a binary image. This technique being based on a proximity rule defined by a structuring element, it could be used successfully for a variety of applications.

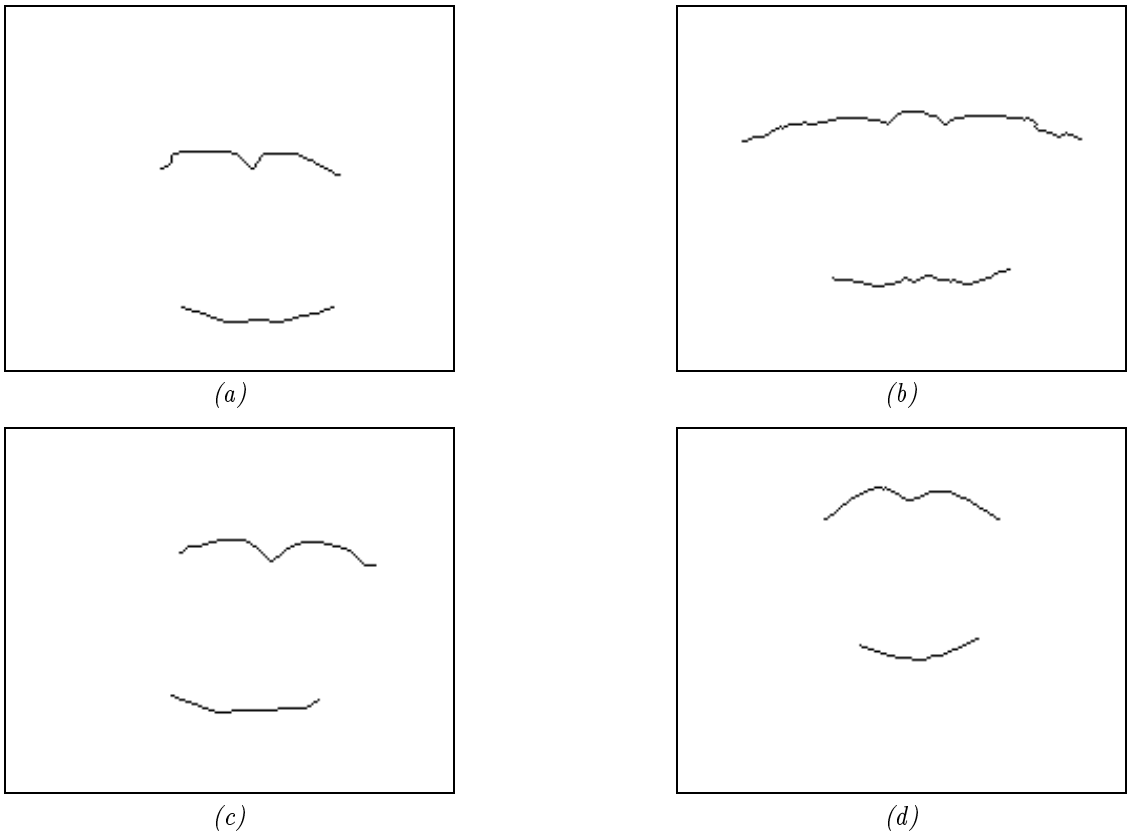

(a) *(b)*

(c) *(d)*

Figure 10 : *Extracted chin/jaw and eyebrow lines.*

7 References

1. R. J. Baron. Mechanisms of human facial recognition. *International Journal of Man Machine Studies*, 15:137–178, 1981.
2. H. Blum. An associative machine for dealing with the visual field and some of its biological implications. In E. Bernard and M. Kare, editors, *Biological Prototypes and Synthetic Systems*, pages 244–260. Plenum Press, New York, 1962. Proc. second Annual Bionics Symposium, Cornell University, 1961.
3. R. Brunelli and T. Poggio. Hyberbf networks for gender classification. In *DARPA Image Understanding Workshop*, San Diego CA, 1992.
4. P. Burt. Smart sensing with a pyramid vision machine. *Proc. IEEE*, 76(8):1006–1015, Aug. 1988.
5. P. Burt. Algorithms and architectures for smart sensing. In *DARPA Image Understanding Workshop*, pages 139–153, Apr. 1998.
6. L. Calabi and W. Harnett. Shape recognition, prairie fires, convex deficiencies and skeletons. Technical Report 1, Parke Math. Lab. Inc., One River Road, Carlisle MA, 1966.
7. L. Farkas. *Anthropometry of the Head and Face in Medicine.* Elsevier, New York, 1981.
8. M. Fischler and R. Elschlager. The representation and matching of pictorial structures. *IEEE Transactions on Computers*, c-22, 1973. Lockheed Palo Alto Research Lab., Lockheed Missiles and Space Company LMSC-D243781, September 1971.
9. M. Fleming and G. Cottrell. Categorization of faces using unsupervised feature extraction. In *International Joint Conference on Neural Networks*, pages 65–70, San Diego CA, June 1990. 2.
10. K. Gabriel and R. Sokal. A new statistical approach to geographic variations analysis. *Systematic Zoology*, 18:259–278, 1969.
11. G. G. Gordon. *Face Recognition from Depth and Curvature.* PhD thesis, Harvard University, Division of Applied Science, Oct. 1991.
12. G. G. Gordon. Face recognition from depth maps and surface curvature. In *SPIE Vol. 1570, Geometric Methods in Computer Vision*, San Diego CA, July 1991.
13. D. Hoffman and W. Richards. Parts of recognition. Memo 732, MIT Artificial Intelligence Laboratory, Dec. 1983.
14. T. Kanade. *Picture Processing by Computer Complex and Recognition of Human Faces.* PhD thesis, Kyoto University, 1973. Department of Information Science.
15. Y. Kaya and K. Kobayachi. *A Basic Study on Human Face Recognition*, pages 265–289. Academic Press, New York, 1972.
16. C. Lantuéjoul and F. Maisonneuve. Geodesic methods in quantitative image analysis. *Pattern Recognition*, 17(2):177–187, 1984.
17. F. Maisonneuve and M. Schmitt. An efficient algorithm to compute the hexagonal and dodecagonal propagation function. In *5th European Congress For Stereology*, pages 515–520, Freiburg im Breisgau FRG, Sept. 1989. Acta Stereologica. Vol. 8/2.
18. R. S. Millman and G. D. Parker. *Elements of Differential Geometry.* Prentice-Hall, New York, 1977.
19. M. Nixon. Eye spacing measurement for facial recognition. In *SPIE Applications of Digital Image Processing VIII*, 1985.
20. M. Schmitt. *Des Algorithmes Morphologiques à l'Intelligence Artificielle.* PhD thesis, Ecole des Mines, Paris, Feb. 1989.
21. M. Schmitt. Variations on a theme in binary mathematical morphology. *Journal of Visual Communication and Image Representation*, 2(3):244–258, Sept. 1991.
22. J. Serra. *Image Analysis and Mathematical Morphology.* Academic Press, London, 1982.
23. J. Serra, editor. *Image Analysis and Mathematical Morphology, Volume 2: Theoretical Advances.* Academic Press, London, 1988.

24. M. Shackleton and W. Welsh. Classification of facial feature for recognition. In *IEEE Int. Computer Vision and Pattern Recog. Conference*, pages 573–579, Maui, HI, June 1991.

25. G. T. Toussaint. The Relative Neighborhood Graph of a finite planar set. *Pattern Recognition*, 12:1324–1347, 1980.

26. M. Turk and A. Pentland. Eigenfaces for recognition. *Journal of Cognitive Neuroscience*, 3(1):71–86, 1991.

27. L. Vincent. *Algorithmes Morphologiques à Base de Files d'Attente et de Lacets: Extension aux Graphes.* PhD thesis, Ecole des Mines, Paris, May 1990.

28. L. Vincent. Efficient computation of various types of skeletons. In *SPIE Vol. 1445, Medical Imaging V*, pages 297–311, San Jose, CA, 1991.

29. L. Vincent. Morphological algorithms. In E. R. Dougherty, editor, *Mathematical Morphology in Image Processing*, pages 255–288. Marcel-Dekker, Inc., New York, Sept. 1992.

30. L. Vincent and D. Jeulin. Minimal paths and crack propagation simulations. In *5th European Congress For Stereology*, pages 487–494, Freiburg im Breisgau FRG, Sept. 1989. Acta Stereologica. Vol. 8/2.

31. L. Vincent, J.-P. Nominé, J. Serra, F. Meyer, J. Arnaud-Battandier, and J.-P. Escande. Cutaneous aging and mathematical morphology. In *Acta Stereologica, Vol. 6/III*, pages 895–900, Caen, France, Sept. 1987. 7th International Congress For Stereology.

32. A. Yuille, D. Cohen, and P. Hallinan. Feature extraction from faces using deformable templates. In *IEEE Int. Computer Vision and Pattern Recog. Conference*, pages 104–109, San Diego, CA, June 1989.